Experimental Techniques
https://doi.org/10.1007/s40799-026-00893-x

RESEARCH PAPER

Experimental Characterization of Flow and Temperature Homogeneity in Standard McKenna Porous Flat Flame Burner

P. Golda[1] · R. Schießl[1] · V. Bykov[1] · N. Ludwig[1] · C. Schmidt[2] · U. Maas[1]

Received: 1 March 2026 / Accepted: 13 May 2026

Abstract

Burners that channel a gaseous methane-air mixture through a porous sintered matrix are widely used to produce flat flames with controlled inlet and boundary conditions. Such environments are essential for studying combustion phenomena and validating physical and chemical models. However, this study shows that even nominally identical McKenna burners with a $25\,\mathrm{mm}$ stainless steel sintered matrix exhibit significant deviations from ideal uniformity. Detailed measurements of the spatial and temporal temperature fields within the matrix, as well as surface flow velocities, reveal substantial non-uniformities: velocity deviations of up to $\pm 50\%$ across the burner surface and temperature differences exceeding $70\,^{\circ}\mathrm{C}$ between center and edge of the matrix. Furthermore, the burner housing temperature increases steadily during operation, reaching over $70\,^{\circ}\mathrm{C}$ after 60 minutes, indicating limited heat removal and pronounced cooling defects. These findings demonstrate that even under nominally steady operating conditions, uniform inflow and boundary conditions cannot be assumed, which is highly relevant for many experimental combustion researchers relying on consistent burner behavior. The results highlight the necessity of accounting for such gradients when using flat flame burners to investigate sensitive combustion phenomena, such as thermo-diffusive instabilities and flame pulsation onset. To facilitate this, the 2D temperature and velocity profiles presented herein can be directly utilized by the community as realistic boundary conditions for future computational fluid dynamics (CFD) simulations of burner-stabilized flames on sintered burners.

Keywords McKenna burner · Premixed flame · Thermal-diffusive instabilities · Experimental investigation

Highlights

(1) Characterization of the gas velocity field after exiting the porous matrix of the McKenna burner reveals spatial inhomogeneities, with local velocity deviations ranging up to ±50%.
(2) Temperature measurements show that the burner housing and porous matrix do not reach thermal steady state even after one hour of operation, with surface temperature differences of up to 70 °C between center and edge.
(3) Limited cooling capacity of the copper coil leads to sustained heat accumulation and challenges in maintaining stable and reproducible thermal boundary conditions.
(4) Underscores the importance of reliable boundary data for studying unsteady combustion phenomena

✉ P. Golda
philipp.golda@kit.edu

1 Institute of Technical Thermodynamics, Karlsruhe Institute of Technology, Kaiserstr. 12, 76131 Karlsruhe, Germany

2 Institute of Fluid Mechanics, Karlsruhe Institute of Technology, Kaiserstr. 10, 76131 Karlsruhe, Germany

Novelty and Significance Statement

This work assesses the ability of two nominally identical McKenna burners to produce burner-stabilized flat flames at well-defined and homogeneous thermal and flow conditions. For this, the flow field, temperature, and cooling conditions of these burners were investigated systematically using a unique combination of hot-wire anemometry, thermocouple measurements, and thermographic imaging, an approach not previously reported in the literature. Furthermore, this study presents the first data on the cooling performance of the integrated copper coil, thereby providing a comprehensive overall picture of the burner performance.

The results evaluate the suitability of the McKenna burner for applications especially involving unsteady and highly sensitive combustion phenomena. Crucially, these findings extend beyond the specific McKenna design, offering the research community a broader basis for assessing experimental data and realistic boundary conditions for sintered matrix burners in general.

Introduction

The so-called McKenna burner [1–6] has been widely used over the past decades to generate flat, premixed flames that are assumed to exhibit an approximately 1-D structure. Its design roots trace back to pioneering work by Botha and Spalding in 1954, who developed a porous burner to measure flame speeds of propane/air mixtures [7]. Unlike pipe flows, where velocity profiles are typically parabolic due to boundary layer effects, porous media should promote more uniform flow distributions by forcing fluids through complex, tortuous paths that suppress large velocity gradients and turbulence. In the literature, there are varying findings regarding flow homogenization through porous media. While [8] confirmed significant homogenization using numerical studies and [9] demonstrated similar results experimentally, other works such as [10] reported local velocity variations of up to $50\,\%$ despite overall homogenization. Especially with respect to hot-wire measurements, such flow profiles in combination with self-convection induced by the wire temperature can lead to increased cooling, which in turn causes a measurement-related overestimation of the actual flow velocities [11, 12].

Building on this foundational concept, the McKenna burner represents a refined and advanced version of the general idea, developed by Holthuis and Associates in the United States during the 1970s [6]. To ensure a uniform temperature distribution across the porous matrix, the design incorporates an integrated cooling coil through which a fluid is circulated. The primary objective of the burner is to establish highly uniform flow and temperature fields, thereby producing a cylindrically symmetric flame. This controlled and well-defined environment significantly facilitates the comparison between experimental data and numerical simulations, which often rely on simplified, reduced-dimensional models. Over the years, the McKenna burner has established itself as a benchmark setup in combustion research, especially for detailed investigations of flame structure and chemistry, as exemplified by the study of Migliorini et al. [1]. This study investigated how “flat” the rich premixed flame produced by the McKenna burner actually is, focusing in particular on the radial uniformity of soot distribution. Their study revealed that while a bronze porous plug results in a significantly more uniform soot profile, the use of a stainless steel plug leads to notable inhomogeneities. These observations raise important concerns regarding the comparability and reproducibility of experimental results obtained with different burner materials. Nevertheless, the stainless steel variant remains a valuable alternative, especially for applications involving higher flame temperatures, such as hydrogen combustion, due to its superior thermal resistance. This highlights a key trade-off: although material modifications expand the burner’s applicability, they may simultaneously introduce variability in flame characteristics, potentially limiting the direct comparability across experimental setups.

In the work from Singh et al. [13] a McKenna burner was used to validate a CFD model. It was shown that the temperature profiles with increasing distance to the burner as well as some of the major species concentrations are showing a good agreement. It should be noted that the McKenna burner was operated within a stable regime, well away from combustion conditions where non-stationary phenomena such as thermal oscillations play a significant role [14]. In such stable operating points, inherent non-uniformities likely remain within acceptable limits where they do not significantly distort global flame characteristics. However, these limits have not been formally quantified in the literature to date.

Campbell et al. [15] investigated rich ethylene/air flames on both a standard McKenna burner and a newly developed compact porous-plug burner, designed for use in spatially constrained diagnostics such as synchrotron facilities. Using Raman thermometry, laser-induced incandescence, and VUV photoionization mass spectrometry, they measured temperature profiles, soot volume fractions, and species concentrations. The study provides valuable kinetic data and shows that the compact burner closely reproduces the flame structure of the standard McKenna setup, confirming its suitability for detailed combustion chemistry and soot studies [3, 16, 17]. Beyond its suitability for detailed diagnostics, the McKenna burner also offers considerable operational flexibility. It can be used with a wide range of fuel–air mixtures and equivalence ratios, making it a versatile tool in combustion research. It is only limited in its application by the flame temperature, as the matrix must be protected from melting.

In most investigations in the literature, the used standard McKenna burner is operated under conditions that produce a stable flame. Consequently, many studies deliberately focus on quasi-steady regimes and avoid parameter ranges that lead to pulsating or cellular flame structures. However, recent advances in combustion science have sparked growing interest in unsteady and transient flame phenomena [14, 18–21], as these dynamic behaviors present valuable opportunities to expand experimental datasets and improve the validation of combustion models. Therefore, in recent years, several research groups have developed custom-built burners inspired by the McKenna design, some involving considerable engineering effort, and employed them as experimental platforms. A particularly noteworthy example is the work by Nechipurenko et al. [22], who investigated diffusive-thermal instabilities in burner-stabilized methane-air flames. Their study combined high-resolution optical diagnostics with numerical simulations to characterize the onset and dynamics of flame oscillations under varying equivalence ratios. This work highlights the complexity of flame behavior even in nominally simple flat flames and underscores the importance of burner design and operating conditions in combustion research.

The growing focus on flame instabilities and transient regimes motivates the development of tailored burner designs and operating strategies that facilitate detailed experimental investigations under such conditions. As a result, there is an increasing demand for comprehensive experimental data capturing these dynamic flame behaviors to validate and refine simulation models, thereby broadening the applicability of McKenna-type burners in fundamental combustion research. Although custom-built McKenna type burners tailored to specific problems are certainly one approach to expanding the experimental database, it is desirable to use a standardized burner design to ensure better comparability of all the data. For this purpose, the standard McKenna burner has become widely established, as previously discussed. However, the cited literature also clearly demonstrates that, especially for complex and highly sensitive phenomena, certain conditions must be met. It is often explicitly assumed that the flow field and the temperature distribution at the burner surface are perfectly homogeneous. Moderate deviations might be tolerable for determining global properties such as the laminar burning velocity. However, they become a critical factor when investigating the onset of local instabilities. In such sensitive regimes, the lack of a defined acceptable limit for non-uniformity in the literature poses a risk, as even minor gradients can break the assumed symmetry. Our results demonstrate that the observed deviations of up to 50% in velocity and $70°C$ in temperature are significantly beyond the thresholds required to justify the common assumption of a quasi-one-dimensional inflow. Studies such as [1] have already shown that certain inconsistencies or ambiguities can arise under less-than-ideal conditions. To date, the literature lacks detailed investigations of the actual boundary and outflow conditions that develop during the operation of the standard McKenna burner. This is precisely where the present paper makes its contribution.

Experimental Setup

The experimental investigation is designed to characterize the operational limits and homogeneity of a standard McKenna burner. To address the complexity of the boundary conditions, the setup is described in terms of its mechanical specifications, fluid supply, and the integrated instrumentation.

Burner Specifications and Geometry

The study utilizes a McKenna burner featuring a stainless steel sintered matrix with a diameter of $25\,\mathrm{mm}$, providing a total surface area of $490.9\,\mathrm{mm}^2$. The porous disc has a thickness of $17\,\mathrm{mm}$ and a nominal porosity of $40.8\,\% \pm 10\,\%$. To minimize the interaction of the flame with the surrounding environment, a bronze shroud ring with an outer diameter of $51\,\mathrm{mm}$ ($2586.9\,\mathrm{mm}^2$) is positioned around the center matrix to provide an inert co-flow. This configuration is representative of the larger $62.6\,\mathrm{mm}$ version, as the manufacturing processes for the sintered matrices are considered analogous.

Fluid Supply and Flow Control

The delivery of gases is managed by a centralized regulation and control system.

- Mass Flow Control: All gas flows are regulated using Bronkhorst EL-FLOW series mass flow controllers. These devices feature a specified accuracy of 0.5% of the reading plus 0.1% of the full scale. By knowing the mass flow rate and the cross-sectional area, the mass flux can be calculated. This parameter is essential to ensure that the investigations remain invariant with respect to the cross-sectional geometry.
- Validation: To further ensure experimental reliability, an independent validation was performed in our laboratory using a bubble flow meter. While the high precision of the certified controllers exceeds the accuracy of manual volumetric measurements, this additional step served as a qualitative 'sanity check' to exclude significant malfunctions or gross deviations, such as errors exceeding 5%. This verification confirmed the integrity of the experimental setup and ensured that the devices operated consistently within their expected performance range.
- Media: For flow homogeneity measurements (Section "Quantifying the Uniformity of the Mean Flow Across the Burner Surface"), dry synthetic air (ALPHAGAZ 1, Grade 5.0) with a purity $\geq 99.999\%$ was used to maintain constant thermophysical properties and prevent sensor fouling due to its low moisture ($H_2O \leq 3\quad \mathrm{ppm}$) and hydrocarbon ($C_n H_m \leq 0.5\quad \mathrm{ppm}$) content.

- Flame Conditions: Combustion studies (Section "Time-Dependent Temperature Evolution of the Burner System" and "Spatial Distribution of Surface Temperature on the Matrix During Burner Operation") were conducted using a premixed methane-air flame at a stoichiometric ratio of $\phi = 1.0$ and a mass flux of $\dot{m} = 0.1\,\mathrm{kg}/(\mathrm{m}^2\mathrm{s})$.

Thermal Management and Instrumentation

To monitor and control the thermal state of the burner during operation, several diagnostic tools are integrated into the setup (see Fig. 1).

- Cooling Circuit: The burner contains an integrated copper coil for liquid cooling [6]. In this study, water was used as the coolant with an inlet temperature of $T_{in} \approx 10°C$ (Section "Time-Dependent Temperature Evolution of the Burner System").
- Burner Housing Temperature: Three Type N thermocouples (TE1, TE2, and TE3) are installed in boreholes at a distance of $1\,\mathrm{mm}$ from the matrix to monitor the temporal evolution of the housing temperature.
- Cooling Performance: The cooling capacity is quantified using Class A PT100 RTDs (accuracy $\pm 0.01°C$) located at the coolant inlet and outlet to measure the temperature difference ΔT_{fluid} (Section "Time-Dependent Temperature Evolution of the Burner System").

Experimental Procedure

The investigation is divided into three primary studies to assess the burner's performance:

- Section "Quantifying the Uniformity of the Mean Flow Across the Burner Surface": Characterization of flow homogeneity across the matrix surface using hot-wire anemometry.
- Section "Time-Dependent Temperature Evolution of the Burner System": Analysis of the time-dependent temperature evolution of the burner housing and cooling power.
- Section "Spatial Distribution of Surface Temperature on the Matrix During Burner Operation": Measurement of the spatial temperature distribution on the matrix surface using thermographic imaging.

Before each investigation, the burner casing was cooled to below $25°C$ to ensure consistent initial conditions for all measurements.

Flow Measurement Technique

The constant temperature hot-wire anemometry (CTA) used in this study falls into the category of thermoelectric velocity measurement method [23, 24]. The method is based on the

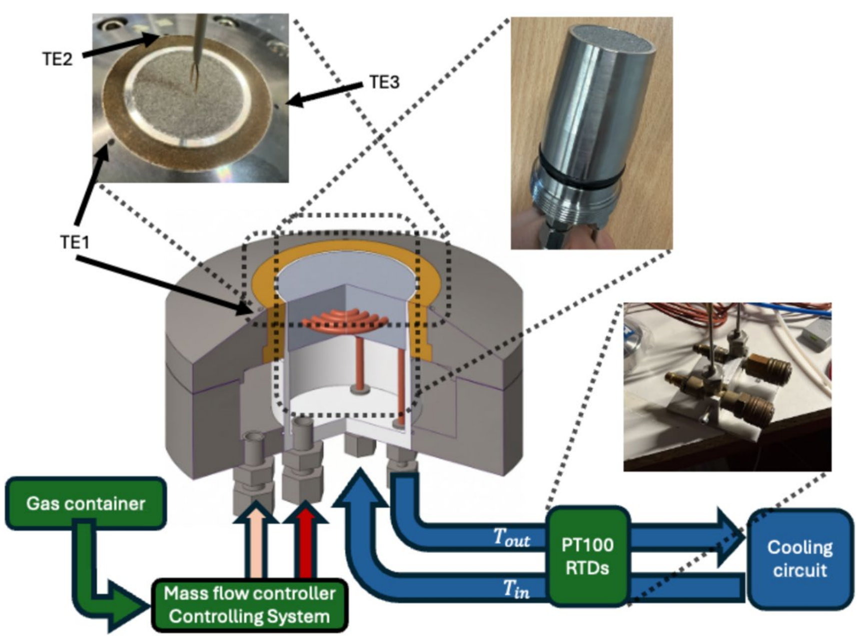

Fig. 1 Sketch of the experimental setup including the position of the used thermocouples (TE). Pink: Co-flow connection, red: Premixed gas connection, blue: Water cooling inlet/outlet

cooling effects of an electrically heated wire, which is placed normal to the main flow direction [24]. The quantity of measure is the heating voltage needed to keep the wire at a defined temperature [24]. The dominant cooling effect is forced convection; other effects such as conduction to the wire support needles are neglected [24]. The electrical resistance of the wire is a function of temperature [24]. Therefore, the heating voltage required to maintain a constant wire temperature is a function of the convective heat transfer, which itself depends on the flow velocity [24]. The CTA used in our study is the DISA TYPE 55M01/55M10 in combination with a Dantec 55P11 miniature wire probe with an overheating ratio of 1.8 and a Type N thermocouple for flow temperature measurements.

Calibration

The calibration of our system was conducted in collaboration with the Institute of Fluid Mechanics (ISTM). We utilized a DISA Type 55D44 Pressure Control Unit combined with a DISA Type 55D45 Nozzle Unit, equipped with a nozzle featuring a 12 mm exit diameter.

Calibration measurements were carried out within a velocity range of approximately $0\,\mathrm{m/s}$ to $7.0\,\mathrm{m/s}$. The voltages measured during calibration were temperature-corrected according to [25]

$$E_{\mathrm{corr}} = E_{\mathrm{meas}} \cdot \left(\frac{T_{\mathrm{w}} - T_{\mathrm{ref}}}{T_{\mathrm{w}} - T_{\mathrm{meas}}}\right)^{n}, \tag{1}$$

where the mean temperature during calibration was used as reference temperature T_{ref}, T_{w} was set to 533K and the temperature correction coefficient n was taken as 0.5, consistent with the standard value used for tungsten wires [23, 24]. To obtain a calibration curve relating the heating wire voltage to flow velocity, a fourth-order polynomial fit was applied to the mean voltage values measured at each calibration velocity (see Fig. 2). This calibration procedure was carried out both before and after the experiment to ensure accuracy and consistency.

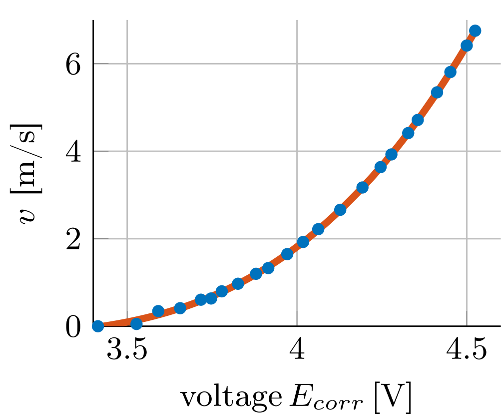

Fig. 2 Calibration Curve

Since the mass flow rate and fluid density were known, the theoretical mean velocity v_{theo} could be calculated. From the 64 measurement points, the mean velocity v_{mean} can be obtained. A comparison of v_{theo} and v_{mean} shows that hot-wire anemometry overestimates the flow velocity up to $100\,\%$ (see ratio r in Table 1). This apparent discrepancy arises from the indirect nature of hot-wire measurements, which depend on the cooling of the wire rather than the velocity alone, because for the heat transfer, the flow topology also plays a major role [24]. Due to the sintered matrix used in the experimental setup, the actual flow at the matrix outlet is expected to be non-uniform in space and potentially turbulent (for more details check next section). In contrast, the calibration was performed under idealized, predominantly laminar conditions, effectively approximating a uniform velocity profile, a scenario that does not reflect the actual measurement conditions. Furthermore, it is also important to note that hot-wire anemometry is expected to show deviations at extremely low flow velocities due to natural convection around the heated wire and heat conduction through the prongs to which the wire is attached. However, despite this mismatch, the general shape of the resulting calibration curve remains applicable for comparative evaluations. The primary difference lies in a voltage offset caused by the differing convective heat transfer coefficients. However, further investigations have shown that v_{theo} becomes valid ($r \approx 1.1 - 1.2$) at a distance greater than 2 cm from the burner surface for all $\dot{V}$, where small-scale flow fluctuations diminish due to viscous damping. To account for the resulting systematic error, the study primarily focused on relative rather than absolute velocity values.

Note from the authors: It should also be emphasized that this paper does not intend to promote or criticize the McKenna burner used. Since the burner has become an established standard tool, the focus of this work is solely on scientifically investigating and assessing its suitability for the study of highly sensitive phenomena. We believe that such an analysis provides significant value to our research and that the findings could be of interest to a broader audience.

Experiment Postprocessing

To obtain the flow field, 64 measurement locations were distributed over the surface within the radius of $12\,\mathrm{mm}$. The

Table 1 Calibration data

$\dot{V}$	$\dot{m} \cdot 10^{-4}$	v_{theo}	v_{mean}	r
[ln/min]	[kg/s]	[m/s]	[m/s]	-
5.00	1.08	0.17	0.20	1.15
7.50	1.62	0.26	0.41	1.57
10.00	2.16	0.34	0.68	1.99
15.00	3.24	0.51	1.12	2.19

specific arrangement of these points, following a polar grid pattern, is illustrated in Fig. 3. This configuration provides near-optimal spacing between the individual points, ensuring excellent spatial coverage across the surface to reconstruct the continuous flow field via linear interpolation. The spacing between measurement locations was approximately $4\,\mathrm{mm}$ in both the radial and tangential directions. It is important to note that the spatial resolution of the CTA system is defined by the dimensions of the wire probe. All measurement data points represent values averaged over the wire length, which is $1.25\,\mathrm{mm}$ in the case of the 55P11 sensor used from Dantec Solutions. This spatial averaging is inherent to the physical operating principle of hot-wire anemometry. The specific $1.25\,\mathrm{mm}$ sensor was selected because preliminary investigations revealed that the characteristic flow structures are spatially coherent over several millimeters. This spatial coherence is a direct consequence of the sintered matrix; its interconnected pore networks cause the flow to emerge in macroscopic zones of predominantly high or low velocity. Since local velocity variations across these zones are gradual rather than abrupt, the chosen wire length accurately captures the flow features without requiring finer spatial resolution. The chosen radial and tangential spacing ensures that individual measurements are independent, with no spatial overlap and minimal flow interaction between adjacent measurement points. To account for temperature drifts, each data point was corrected using the local flow temperature (T_{meas}) recorded during the measurement. This procedure normalizes the measured voltages to the reference temperature of the calibration (T_{ref}) using Eq. (1). Since both the calibration and the actual experiments were conducted using the same dry synthetic air under identical environmental conditions ($T_{\mathrm{meas}} \approx T_{\mathrm{ref}}$), this correction is strictly speaking optional. Nevertheless, it was systematically applied to all data points to eliminate even residual thermal drifts and ensure the highest possible measurement accuracy. Subsequently, the corrected heating voltage is converted to flow velocity using the previously established calibration curve.

Results

Quantifying the Uniformity of the Mean Flow Across the Burner Surface

As mentioned in the introduction, the burner is frequently used to experimentally represent a 1-D flame. For this purpose, it is essential that the flow field is uniformly distributed across the cross-section. Since the burner employs a sintered matrix, it is possible that local variations of the velocity field may occur. These variations can influence the results or, in extreme cases, even invalidate the assumption of a 1-D structure.

For the investigation of homogeneity, the overall volume flow rate $\dot{V}$ was varied for a cold air flow. The tested values ranged from 5 to $15\,\mathrm{ln/min}$. The volume rates were selected since these are of the same order of magnitude as in the investigation of methane-air flames using the 25 mm McKenna burner. The measured velocity values v are illustrated in an image plot in Fig. 3. Therefore, the measured data were interpolated linearly to a 100x100 mesh, which facilitates visualization the flow field easily. In addition, Fig. 4 shows the corresponding relative velocity deviation $v_{\mathrm{p}} = (v - v_{\mathrm{mean}})/v_{\mathrm{mean}} * 100$.

It is evident that the velocities deviate considerably from the mean, indicating a noticeable inhomogeneous flow. The pattern that emerges appears quite similar across all three flow rates, suggesting that it is unlikely to change significantly for lower or also higher flow rates. It is worth noting that points with a $+50\%$ deviation show a flow velocity that is 200% higher than points with a -50% deviation. Such a flow field deviates significantly from a cylindrically symmetric profile and, at first glance, appears quite surprising. Furthermore, no distinct pattern in the velocity distribution is apparent; the distribution seems random, without any clear structure (e.g., faster in the center, slower at the edges). While some degree of variation was expected based on the sintering process,

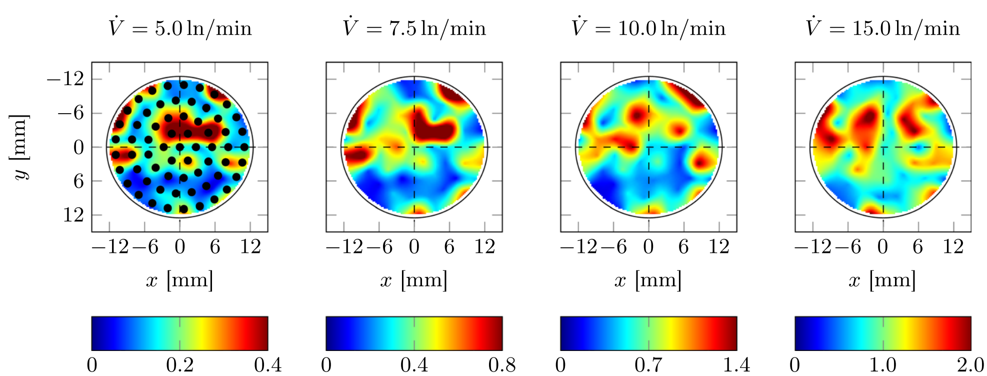

Fig. 3 Measured absolute velocity values v in [m/s] for matrix M1. The 64 measurement points are shown for reference only in the left plot

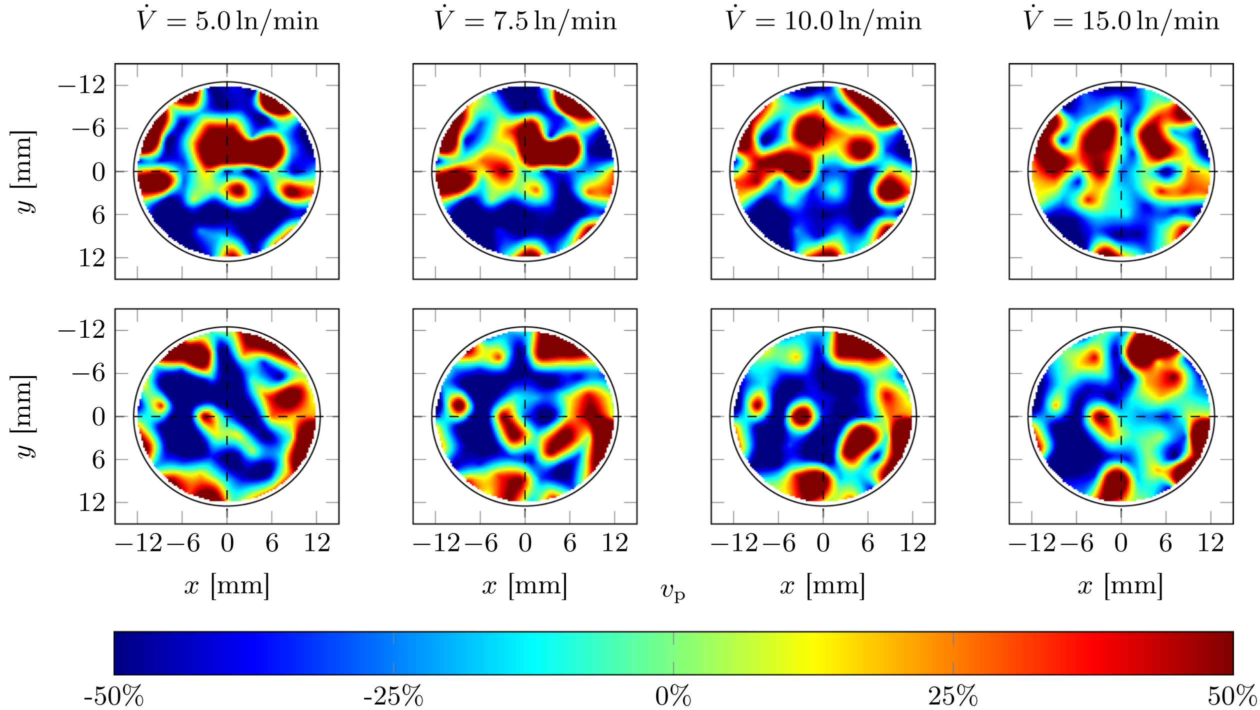

Fig. 4 Relative deviation from the mean flow velocity for M1 (upper row) and M2 (lower row). The data shown are the interpolated values based on the 64 measurement locations

its magnitude was unforeseen. Given these unexpected flow profiles, we contacted the manufacturer to discuss our findings. In response, they provided us with a second matrix (M2), which we installed to repeat the measurements. The results are shown in the bottom row of Fig. 4. It can be seen that significant differences in flow velocity are also present here. Based on the pattern, no similarities to M1 can be derived. While the exact reason for this cannot be definitively determined, it is reasonable to assume that the sintering-based manufacturing process of the matrices leads to differences in its structure and thus influencing their flow characteristics. According to the manufacturer's specifications, the porosity of the sintered matrix lies within the range of $38 - 43\,\%$, with a manufacturing tolerance of $\pm 10\,\%$. This confirms that approximately $40\,\%$ of the volume consists of void space (pores), while the remaining $60\,\%$ is solid material. In general, however, we believe that this is less related to the manufacturer itself and more a result of the matrix production process. Therefore, it can be expected that each matrix exhibits a different flow field, which may cause the results to deviate to some extent. These velocity inhomogeneities are expected to significantly influence the flame structure, especially under sensitive conditions. The observed deviations contradict the commonly assumed one-dimensional inflow field of McKenna burners, suggesting that the flame cannot be considered quasi-1D in this configuration.

Time-Dependent Temperature Evolution of the Burner System

For reproducible results, it is crucial that thermal conditions of the burner are constant over time. As already mentioned, the burner has no manufacturer-provided details on the required flow rate, medium, or temperature for cooling. Therefore, the volume flow rate of water ($T_{\mathrm{water}} \approx 10\,°\mathrm{C}$) was varied to check its influence. A steady-state equilibrium is established through the interplay of heat conduction, radiation, and convective cooling via the coil. Since the matrix surface has the most significant influence on flame behavior, three Type N thermocouples (TE1–TE3, see boreholes in Fig. 1) were positioned at a distance of 1 mm to the matrix. These thermocouples monitor the temporal evolution of the burner housing temperature starting from room temperature (t = 0 s), allowing us to determine whether a steady-state temperature has been reached or not. The profiles are plotted in Fig. 5. It is observed that the temperature increases from room temperature to approximately 70°C within 2 hours. Based on this, it can be concluded that the integrated cooling coil is unable to remove as much energy as is induced into the burner by the flame. This can be explained with the upper right photo in Fig. 1. A part of the heat transfer out of the burner is through the burner housing. The observed effect is a direct result of the 2 mm metal ring located between the burner matrix and the co-flow matrix. The ring enhances

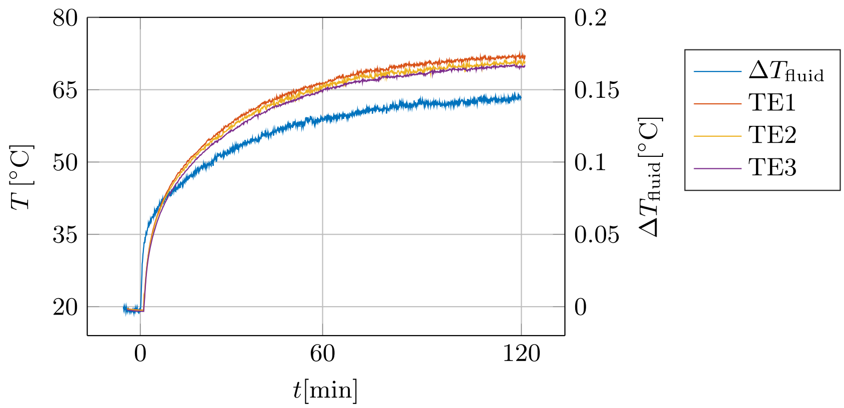

Fig. 5 Burner housing temperatures over two hours from ambient at $t = 0$, with the cooling fluid $\Delta T_{\mathrm{fluid}}$ shown for reference

cooling by promoting heat transfer within the burner housing. Consequently, the issue arises from the burner's design and cannot be avoided at the current stage. However, it should be noted here that the displayed T, t curve continues to rise even after 1 hour of operation, which makes it difficult to conduct reproducible investigations without spending hours of preheating the burner.

As already mentioned, the essential function of the cooling coil is to effectively dissipate heat from the matrix. However, the last paragraph has shown that the burner heats up over time. This indirectly implies that the burner's cooling capacity has to be lower than the energy absorbed by heat conduction and thermal radiation from the flame. To determine the cooling capacity, the temperature of the coolant was monitored using Class A PT100 RTDs (accuracy $\pm 0.01\,°\mathrm{C}$) positioned immediately upstream of the inlet and downstream of the outlet. While the incoming water at $T_{\mathrm{in}} = 10\,°\mathrm{C}$ exhibited supply fluctuations of approximately $\pm 0.5\,°\mathrm{C}$, these variations are negligible for the overall heat dissipation analysis due to the very large temperature gradient between the burner surface and the coolant. If the temperature difference $\Delta T_{\mathrm{fluid}} = T_{\mathrm{out}} - T_{\mathrm{in}}$ between the inlet and outlet is known (see Fig. 6(a)), the cooling power can be calculated based on the known volume flow rate $\dot{V}$ and density ρ (see Fig. 6(b)) of the coolant. The results in Fig. 6(b) show that the average cooling power increases with rising volumetric flow rate at first, before staying at a nearly constant value for the higher $\dot{V}$ values. It is also interesting to note that the cooling power nearly doubles between 5 and 60 minutes, despite the fact that the matrix temperatures do not change significantly beyond 5 minutes (see next section for more details). This suggests that the increase in $\dot{Q}$ is caused by the heating of the burner housing, which contradicts the intended function of the cooling mechanism, namely the efficient cooling of the burner's sintered matrix. Comparative one-dimensional simulations of a burner-stabilized flame were conducted for the given geometry and a burner surface temperature of $T = 75\,°\mathrm{C}$ using the established in-house code INSFLA. In this 1-D model, the spatial coordinate (denoted as z in the following) strictly represents the axial distance normal to the burner surface. These simulations indicate a conductive heat input into the burner of approximately 30 W. While the primary focus of this work is not on numerical analysis, further details on the code can be found in literature [26–31]. However, for better visualization, Fig. 7 presents the stationary

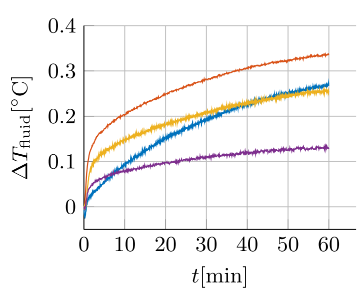

(a) Temperature difference $\Delta T_{\mathrm{fluid}}$ between the fluid entering and leaving the burner over time.

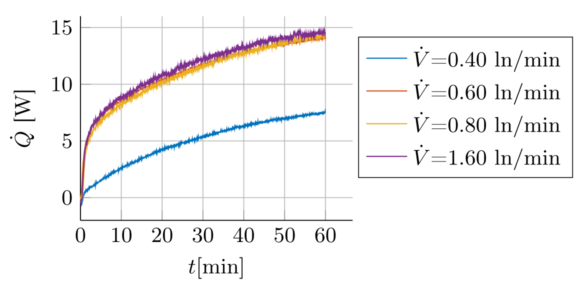

(b) Cooling power of the fluid over time.

Fig. 6 Thermal characteristics of the fluid flow during operation

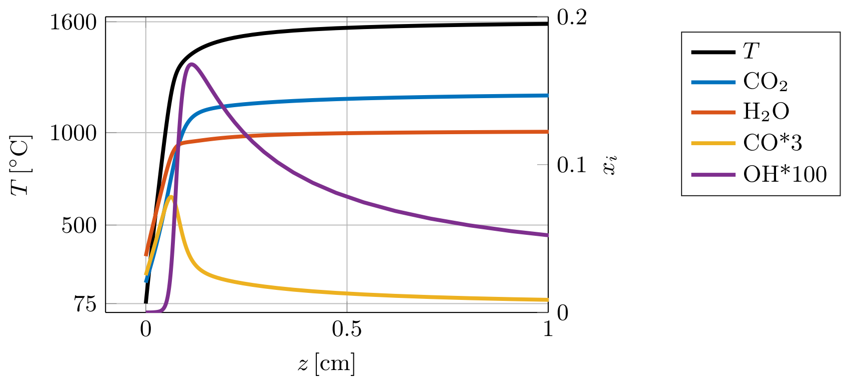

Fig. 7 Simulated profiles of temperature T and species mass fractions x_i over the axial distance z from the burner surface. Selected mass fractions are scaled for better visibility

flame profiles of temperature and selected mass fractions x_i. Owing to the solver's grid control, the temperature gradient is obtained with high accuracy, lending credibility to the calculated heat flux of about 30 W. This seems reasonable, considering that even after one hour of operation, the cooling power continues to increase, indicating a further rise in burner temperature.

In summary, it can be stated that the cooling performance is lower than the energy input from the flame, causing the burner to heat up over time. This behavior is far from ideal and significantly complicates the establishment of constant boundary conditions.

Spatial Distribution of Surface Temperature on the Matrix During Burner Operation

As fuel/air mixture flows through the pores of the burner matrix, heat transfer between the gas and the matrix will occur. The temperature field on the burner matrix, therefore, directly influences the temperature of the unburned gas flowing into the flat flame and thus the flame behavior. To experimentally assess the matrix surface temperature, a thermographic camera (InfraTec ImageIR 9400 HP with a 100 mm telephoto lens and close-up adapter) with a spatial resolution of 739x795 pixels across the measurement area was employed. To determine the emissivity ε of the matrix, a calibration sample was prepared. Thermography results were checked against point-wise thermocouple measurements. With an emissivity of $\varepsilon = 0.55$ the agreement found was within $< 5\,\mathrm{K}$. This value was subsequently used in further measurements. Additionally, literature supports this finding, with reported emissivities in the range $\varepsilon = 0.4 - 0.6$ for rough stainless steel surfaces [32–35]. For all investigations, the following procedure was used: The burner is operated in the usual way for a certain duration in time ("operation time"). With the flame sitting on the burner matrix, thermographic measurements of matrix temperature are plagued by interference with hot flame gases. Because thermography cannot be performed with an active burner, at some defined point in time (defined as 0 ms), the flame is blown out to allow unobstructed thermographic view onto the burner matrix. For about 200 ms after this, hazes of burned exhaust gas from the flame are still visible in the thermography images (see frame "200 ms" in Fig. 8). After 300 ms, no more evidence of remaining hot flame gas is observed; the recorded temperature data now are solely burner surface temperatures. Throughout the entire procedure, even after flame extinction, the cooling loop remained in continuous operation. Within the extremely short measurement window of 300 ms, instantly stopping the cooling water flow is simply impossible due to the inertia of the coolant. However, this does not substantially alter the final results anyway.

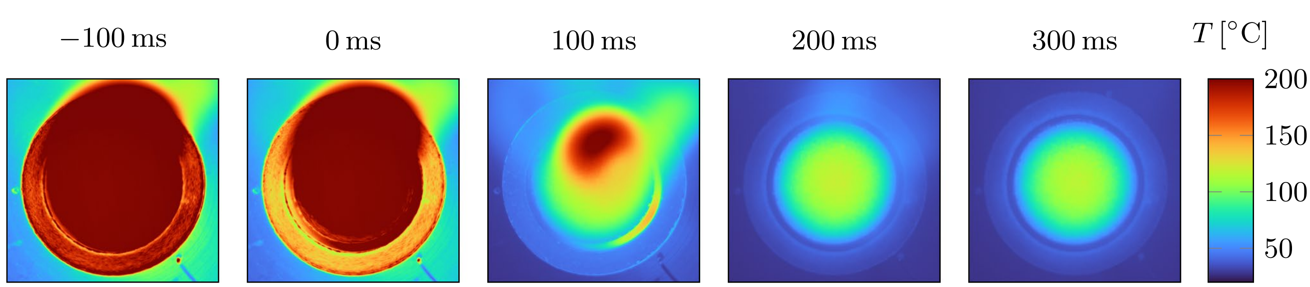

Fig. 8 Time-resolved thermographic snapshots of the burner matrix during and after flame blowout. The images show the spatial temperature distribution across the matrix surface at selected time points

It is important to note that the temperature measured at 300 ms does not directly represent the temperature during active burner operation. In order to illustrate this, Fig. 9(a) presents $T(t)$ at the burner's center point for the case of 300 s operation time. The data was fitted using a double-exponential function of the form

$$T(t) = T_\infty + A_1\, e^{-t/\tau_1} + A_2\, e^{-t/\tau_2}, \tag{2}$$

where T_∞ is the asymptotic temperature, A_1 and A_2 are the amplitudes of the relaxation processes, and τ_1 and τ_2 are the corresponding time constants. This approach captures both the rapid thermal conduction within the burner plug normal to the burner surface as well as the radial thermal conduction. Note that natural convection and radiation are playing a minor role in the cooling process. This was demonstrated by comparing the cooling curves in two cases: (a) flame extinction by blowing, the premixed gas still flowed out of the matrix during cooling (b) flame extinction by blowing, no gas flow during cooling (see Fig. 10) (c) flame extinction by interrupting the fresh-gas supply, no gas flow during cooling. The two cooling curves were indistinguishable; no significant enhancement of cooling due to the cold outflowing gas was observed.

The fit allows extrapolating the data from 300 ms back to 0 ms to evaluate whether considering the temperatures at 300 ms is reasonable. For the case considered, the deviation between 0 and 300 ms based on the fitted data is $\approx 10\,°\mathrm{C}$. In comparison, the measured temperature change from 300 ms to 600 ms is 5.9 °C. Nevertheless, both comparisons confirm that the matrix temperature of the porous plug is not significantly higher than the value shown at 300 ms, which is therefore used as the representative value in the following.

The burner operation time, and consequently the duration of heat input from the flame, was varied between 30s and 300s. Figure 10 depicts the matrix temperature results after a predefined burning period. Although the burner housing temperature increased significantly during continuous operation, its effect on the matrix temperature was minor, and no significant temperature differences were observed for durations longer than $250 - 300$ s. For this reason, the temperature distribution after 300 s can be considered as the steady-state temperature distribution of the matrix. To ensure consistency across measurements, the casing was cooled to below 25°C before each test, thereby maintaining nearly identical initial conditions. Each configuration was tested four times. The results show that the matrix temperatures are significantly correlated with the burn duration.

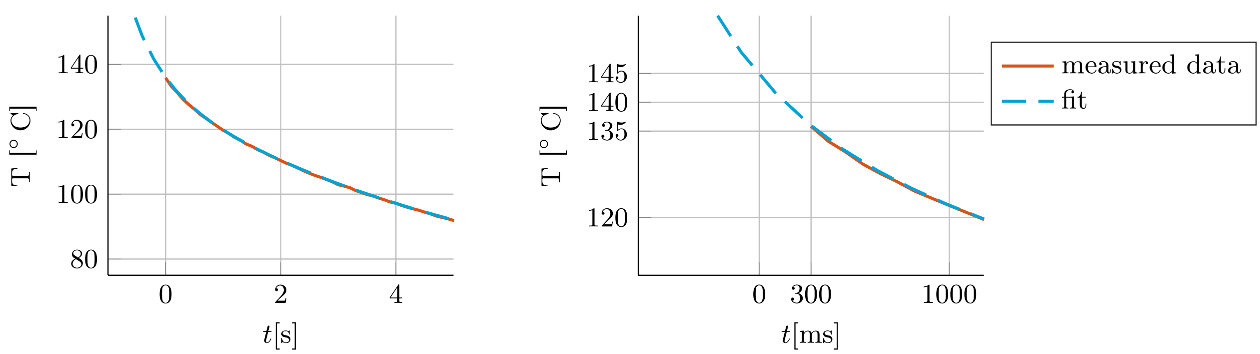

(a) $T(t)$ for the first 5 seconds.

(b) Zoomed view highlighting the extrapolation.

Fig. 9 *T,t* cooling curve for the porous matrix center point

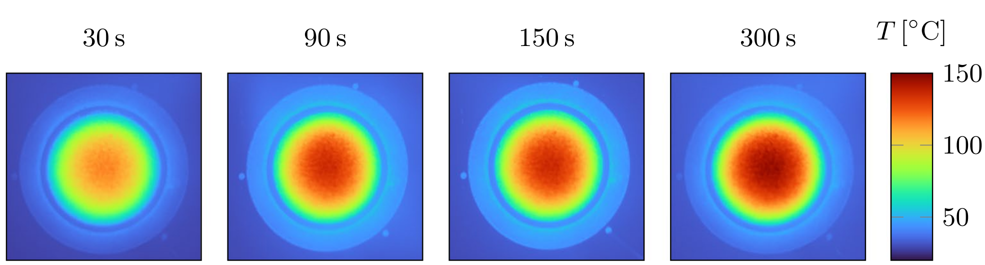

Fig. 10 Spatial temperature distribution of the burner matrix recorded 300 ms after flame blowout, following prior operation durations of 30, 90, 150, and 300 seconds

Furthermore, depending on the maximum temperatures that occur in the center of the matrix, larger gradients are observed across the burner matrix.

To illustrate the profiles in an easier way, Fig. 11 presents the temperature profiles along the horizontal and vertical centerlines of the burner for the 30 s case. The plot clearly demonstrates the symmetry of the temperature distribution and marks the boundary between the matrix and the adjacent 2 mm plates. Figure 12 shows, analogous to Fig. 11, the profiles through the center for 90, 150, and 300 s burning time. Here too, symmetry is clearly evident, although the curves slightly lean to the right. This can potentially be explained by the position of the cooling coil inside the matrix. However, it is noticeable here that there is a temperature difference of approximately 70°C between the center and the outer points of the matrix. As explained in the previous section, it is clearly evident that the 2 mm thick metal ring, which separates the inner matrix from the co-flow matrix, strongly supports cooling through heat conduction within a solid due to its robust construction. Spatial variations in temperature are intensified by this design, as the dominant mode of this heat transfer is radial rather than perpendicular to the surface. Furthermore, this provides a plausible explanation for why the burner housing heats up to over 70°C with increasing burn duration. In simple words: the cooling coil cannot sufficiently compensate for the continuous heat input from the flame.

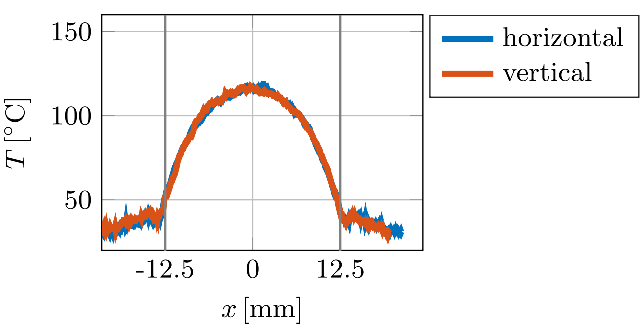

Fig. 11 Temperature distribution through the burner center after flame extinction (30 s operation time)

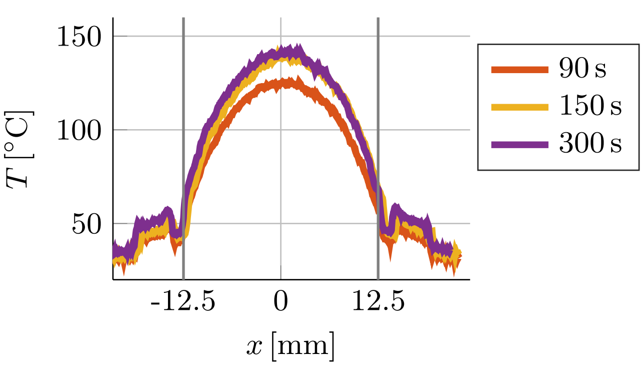

Fig. 12 Temperature distribution through the burner center after flame extinction (90, 150, 300 s operation time)

Summary and Conclusions

This work investigates the operational characteristics of the standard McKenna burner used for premixed methane–air flames. The primary focus is on the velocity field of the gas flow after it exits the porous matrix, as this defines the actual inflow conditions for the flame. In addition, the temperatures of both the burner housing and the porous matrix during operation are analyzed to comprehensively characterize the key boundary conditions affecting flame behavior. Accurate knowledge of these inflow conditions is essential for studying specific flame phenomena, particularly highly sensitive unsteady processes such as thermo-diffusive flame oscillations, which are currently of significant research interest.

Initial investigations revealed partially unexpected results. Most notably, the burner required an unexpectedly long time to reach thermal steady state. Temperature measurements showed that even after one hour of operation, the burner temperature continued to rise. The primary cause was identified as the limited cooling capacity of the installed copper coil, which was insufficient to balance the heat input from the flame. Furthermore, the cooling performance was found to vary with the volumetric flow rate, complicating efforts to maintain stable thermal boundary conditions and, consequently, to ensure reproducibility of experiments. In addition, the inflow velocity fields exhibited significant inhomogeneities across the burner matrix surface, particularly in one of the two investigated matrices. For this matrix, local deviations of approximately 50% relative to the mean velocity were observed. In contrast, the second (nominally identical) matrix showed lower but still notable deviations with a totally different structure. Similarly, the surface temperature distribution of the burner revealed a characteristic non-uniform pattern, with temperature differences of up to 70°C between the matrix center and its outer edge. These findings raise the question of whether the flame configuration can genuinely be considered quasi-one-dimensional under such conditions.

Motivated by these findings, future work will focus on the development of a novel research burner designed to specifically address these limitations. The primary design objectives for this new system are active thermal management, highly homogeneous flow conditions, and improved accessibility for measurement techniques. While a rigorous characterization is beyond the scope of the present study, a

(a) McKenna burner

(b) Own prototype

Fig. 13 Comparison of the produced flat methane-air flames

first prototype, sharing the same macroscopic dimensions and nominal porosity as the investigated McKenna burner, has already been built. Figure 13 provides a qualitative visual outlook, showing a flat methane-air flame stabilized on this initial prototype alongside the McKenna burner M1. A comprehensive evaluation and a detailed performance comparison between the two designs will be the subject of future publications.

In summary, the results highlight the importance of carefully assessing the actual boundary conditions when using the McKenna burner for flame diagnostics. While the burner performs reliably for studying stable flames far from instability thresholds, its suitability must be critically evaluated for highly sensitive phenomena. In such cases, significant temperature and velocity gradients may compromise the validity of the inferred flame properties and limit the reproducibility of experimental results.

Author Contributions Philipp Golda: Conceptualization, Data curation, Investigation, Methodology, Validation, Visualization, Writing - original draft, Writing- review & editing Robert Schießl: Formal analysis, Investigation, Methodology, Supervision, Writing- review & editing Viatcheslav Bykov: Investigation, Methodology, Visualization, Writing- review & editing Niklas Ludwig: Investigation, Writing- review & editing Carola Schmidt: Investigation, Writing- review & editing Ulrich Maas: Resources, Supervision, Writing- review & editing

Funding Open Access funding enabled and organized by Projekt DEAL.

Declarations

Conflicts of Interest The authors declare that they have no known competing financial interests or personal relationships that could have appeared to influence the work reported in this paper.

Generative AI in Scientific Writing During the preparation of this work, the authors used the ChatGPT-4 model to assist with spelling, grammar correction as well as tikz programming. After using this tool/service, the authors reviewed and edited the content as needed and takes full responsibility for the content of the publication.

References

1. Migliorini F, Deiuliis S, Cignoli F, Zizak G (2008) How “flat” is the rich premixed flame produced by your McKenna burner? Combust Flame 153:384–393
2. Tran L-S, Glaude P-A, Fournet R, Battin-Leclerc F (2013) Experimental and modeling study of premixed laminar flames of ethanol and methane. Energy Fuel 27:2226–2245
3. Xu F (1997) Soot formation in laminar premixed ethylene/air flames at atmospheric pressure. Combust Flame 108:471–493
4. Jiang L, Wu Y, Zhou G, Li X (2023) Experimental study on the instability characteristics of CO2-diluted n-butane/air cellular flames on McKenna burner. Exp Therm Fluid Sci 143:110846
5. Jin W, Wang J, Nie Y, Yu S, Huang Z (2015) Experimental study on flame instabilities of laminar premixed CH4/H2/air non-adiabatic flat flames. Fuel 159:599–606
6. Holthuis L (2025) About Flatflame. https://www.flatflame.com/about-flatflame
7. Botha JP, Spalding DB (1954) The laminar flame speed of propane/air mixtures with heat extraction from the flame. Proc R Soc London Ser A Math Phys Sci 225:71–96
8. Lasseux D, Valdés-Parada FJ, Thovert J-F, Mourzenko V (2021) Exuding porous media: Deviations from Darcy's law. J Fluid Mech 911:A48
9. Arthur J (2020) PIV study of flow through and over porous media at the onset of inertia. Adv Water Resour 146:103793
10. Rashidi M, Peurrung L, Tompson A, Kulp T (1996) Experimental analysis of pore-scale flow and transport in porous media. Adv Water Resour 19(3):163–180
11. Feng Z, Ye Q (2023) Turbulent boundary layer over porous media with wall-normal permeability. Phys Fluids 35(9):095111
12. Silin N, Cuscueta D, Clausse A (2021) Experimental assessment on the performance of hot wire anemometry in and around a permeable medium by comparison with Particle Image Velocimetry. Flow Meas Instrum 78:101827
13. Singh KD, Gangadharan P, Chen DH, Lou HH, Li X, Richmond P (2014) Computational fluid dynamics modeling of laboratory flames and an industrial flare. Japca J Air Waste Ma 64:1328–1340
14. Gubernov V, Bykov V, Maas U (2017) Hydrogen/air burner-stabilized flames at elevated pressures. Combust Flame 185:44–52
15. Campbell MF, Schrader PE, Catalano AL, Johansson KO, Bohlin GA, Richards-Henderson NK, Kliewer CJ, Michelsen HA (2017) A small porous-plug burner for studies of combustion chemistry and soot formation. Rev Sci Instrum 88:125106
16. Salaün E, Frindt F, Cabot G, Renou B, Richard S, Cazalens M, Malbois P, Grisch F (2020) Experimental investigation on NO pollutant formation in high-pressure swirl-stabilized kerosene/air flames using NO-, OH- and Kerosene-PLIF and PIV laser diagnostics. In: Volume 4A: Combustion, Fuels, and Emissions,

American Society of Mechanical Engineers, Virtual, Online, p V04AT04A052
17. Maricq M, Harris SJ, Szente JJ (2003) Soot size distributions in rich premixed ethylene flames. Combust Flame 132:328–342
18. Gubernov V, Kolobov A, Bykov V, Maas U (2016) Investigation of rich hydrogen-air deflagrations in models with detailed and reduced kinetic mechanisms. Combust Flame 168:32–38
19. Bykov V, Gubernov V, Maas U (2018) Mechanisms performance and pressure dependence of hydrogen/air burner-stabilized flames. Math Model Nat Phenom 13:51
20. Korsakova A, Gubernov V, Kolobov A, Bykov V, Maas U (2016) Stability of rich laminar hydrogen-air flames in a model with detailed transport and kinetic mechanisms. Combust Flame 163:478–486
21. Moroshkina A, Sereshchenko E, Mislavskii V, Gubernov V, Minaev S (2024) Study of chemiluminescence of methane-air flame stabilized on a flat porous burner. Combust Flame 270:113755
22. Nechipurenko S, Miroshnichenko T, Pestovskii N, Tskhai S, Kichatov B, Gubernov V, Bykov V, Maas U (2020) Experimental observation of diffusive-thermal oscillations of burner stabilized methane-air flames. Combust Flame 213:202–210
23. Niesiołowski-Gawin VV (2006) Geschwindigkeitsmessung. In: Strömungsmesstechnik, Springer-Verlag, Berlin/Heidelberg, pp 41–78
24. Örlü R, Vinuesa R (2017) Thermal anemometry. In: Discetti S, Ianiro A (eds) Experimental Aerodynamics, 1st edn. CRC Press, Boca Raton, CRC Press, 2017, pp 257–304
25. Hultmark M, Smits AJ (2010) Temperature corrections for constant temperature and constant current hot-wire anemometers. Meas Sci Technol 21(10):105404
26. Maas U, Warnatz J (1988) Ignition processes in hydrogen oxygen mixtures. Combust Flame 74:53–69
27. Moroshkina A, Mislavskii V, Kichatov B, Gubernov V, Bykov V, Maas U (2023) Burner stabilized flames: Towards reliable experiments and modelling of transient combustion. Fuel 332:125754
28. Goyal G, Maas U, Warnatz J (1995) Simulation of the Behavior of Rich Hydrogen-Air Flames Near the Flammability Limit. Combust Sci Technol 105:183–193
29. Maas U (2006) Combustion. Springer, Berlin Heidelberg
30. Maas U, Warnatz J (1989) Simulation of chemically reacting flows in two-dimensional geometries. Comput Sci Eng 394–420
31. Luo Y, Strassacker C, Ferraro F, Zentgraf F, Dreizler A, Maas U, Hasse C (2022) A manifold-based reduction method for side-wall quenching considering differential diffusion effects and its application to a laminar lean dimethyl ether flame. Int J Heat Fluid Fl 97:109042
32. Sih SS, Barlow JW (2004) The prediction of the emissivity and thermal conductivity of powder beds. Particul Sci Technol 22:427–440
33. Taylor S, Wright JB, Forrest EC, Jared B, Koepke J, Beaman J (2020) Investigating relationship between surface topography and emissivity of metallic additively manufactured parts. Int Commun Heat Mass 115:104614
34. Terrazas-Nájera CA, Fernández A, Felice R, Wicker R (2024) On the thermal emissive behavior of four common alloys processed via powder bed fusion additive manufacturing. Addit 82:104023
35. Cao G, Weber S, Martin S, Anderson M, Sridharan K, Allen T (2012) Spectral emissivity measurements of candidate materials for very high temperature reactors. Nucl Eng Des 251:78–83